Tomographic reconstruction of the void distribution in the nuclear fuel test loop FRIGG

Karin Holmquist

Thesis for the Master of Science degree
The Department of Nuclear and Particle Physics, Uppsala University

Abstract

A non-destructive tomographic measurement technique is used at the nuclear fuel test loop FRIGG, owned by Westinghouse Electric Sweden AB in Västerås. The technique is used for making measurements of the void distribution, i.e. the distribution of steam and water, in a mockup of a nuclear fuel assembly. When performing a measurement at FRIGG, gamma radiation is transmitted from a Cs-137 source through the fuel assembly to be detected on the opposite side. The detected gamma intensities are used to reconstruct images of the void distribution inside the assembly.

The reconstructions have earlier been done using an analytical reconstruction technique. In the present work, the possibility to increase the resolution and the precision of the reconstructed images by using an algebraic reconstruction technique has been investigated. By using this technique, consideration has been taken to known geometries and materials in the assembly, such as the fuel rods and the surrounding pressure vessel. The influence of the well-known objects on the measured data has been corrected for, enabling the exclusion of these regions from the reconstructions. The idea has been that this technique would imply improved precision and resolution of the regions of interest, which is the distribution of steam and water between the rods. Reconstructions have been made both using measured data from FRIGG measurements and simulated data. The algebraic reconstruction technique has been applied but without resulting in significant improvements as compared to earlier results.

However, another way of performing the measurements using a set of measured reference intensities has been suggested. Simulations of such measurements have been made with very promising results.

Contents

1 Introduction

1.1 Nuclear fuel assemblies

In a nuclear power plant, uranium is used as fuel. The uranium is encapsulated in rods, which are organized together in four sub bundles in fuel assemblies and surrounded by water. In this work, the SVEA-96S fuel type, consisting of 96 rods organized in four sub bundles, has been considered. This assembly is illustrated in Figure 1.1.

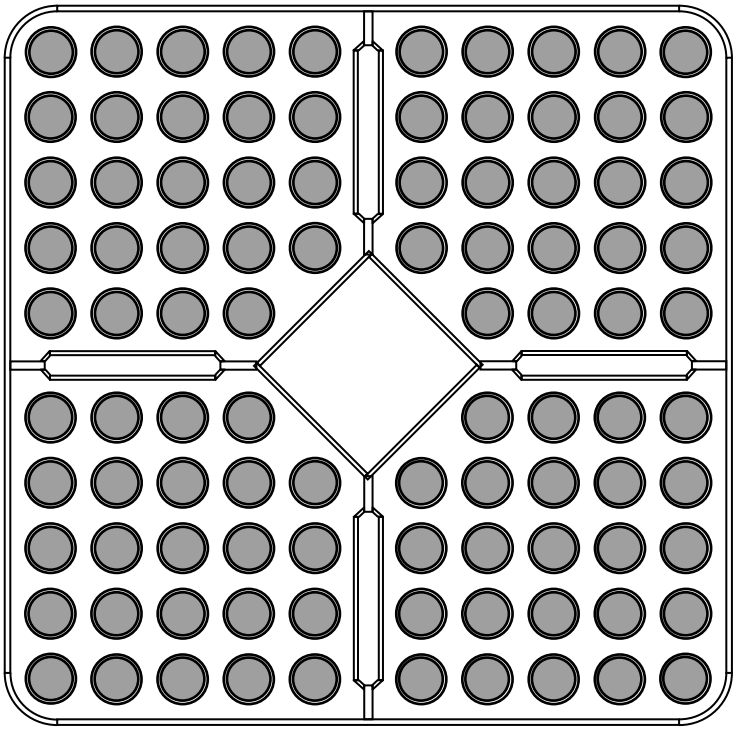

Figure 1.1. An axial cross section of a fuel assembly of type SVEA 96-S.

1.2 Void

The distribution of steam and water, also called the void, is an important control factor in a fuel assembly. The water surrounding the rods works as a transporter of heat. As the rods are warmed up by the power from the fission reactions taking place in the reactor, heat needs to be transported out of the rods in order to keep them from getting over heated. An over heated fuel rod will be subject to dry-out, an incident which would cause serious damage to the rod. Hence it is important that, at all times while the system is running, there is water surrounding the rods. Accordingly, supervising the void level is of great importance.

The void also plays another important role as a means to control the power level in a boiling water reactor. The fission reactions are kept under control in different ways, one of them is by controlling the void. Neutrons traveling through water are slowed down to a higher extent than neutrons traveling through steam. This means that in a reactor containing a large amount of steam, i.e. with a high void rate, neutrons have a higher energy. Consequently, they are less likely to interact with nuclei and hence the reaction rate is limited.

2 Tomographic measurements at the FRIGG test loop

In this work, data from measurements performed on a mockup of a sub bundle of the SVEA-96S type have been analysed. The measurements were made in the test loop FRIGG at Westinghouse Electric Sweden AB in 1998.

2.1 Transmission tomography

Transmission tomography is a non-destructive measuring technique where highly energetic ionizing radiation is used to obtain sectional images of objects. The radiation is emitted on one side of an object and is detected on the opposite side. Depending on the characteristics of the material of the object, it is attenuated to a certain extent. The denser the material, the more the ray is attenuated. If the number of measurement points is sufficient enough, an image of the attenuation in the object can be reconstructed from the detected intensities.

2.2 The FRIGG loop

FRIGG is a thermal-hydraulic test loop for nuclear fuel assemblies, owned by Westinghouse Electric Sweden AB, former ABB Atom, in Västerås. The test loop is illustrated in Figure 2.1. It was finished in 1966 and makes it possible to perform tests of full-scale assemblies as well as sub bundles, ref. [1]. In this work, FRIGG measurements on one single bundle have been used. The test rods in FRIGG are electrically heated to simulate the heating from the fission reactions taking place in a real reactor. The heated rods warm up the water surrounding the rods and steam is created. The steam/water distribution can then be investigated and from this, more can be learnt about the behaviour of the void. This knowledge can be used to prevent dry-out from happening to real fuel rods.

At the FRIGG test loop, there is a tomographic measuring equipment for obtaining images of the void distribution in the fuel mockup. The equipment is also included in Figure 2.1.

Figure 2.1. Positioning of the tomographic measuring equipment about the test loop FRIGG. Reproduced by courtesy of Westinghouse Electric Sweden AB.

2.3 Applications of tomographic techniques for void measurements in FRIGG

Measurements of the steam/water distribution, or void, have been made at FRIGG using transmission tomography. This type of measurement is performed by transmitting gamma radiation from a Cesium-137 source, through the fuel assembly, to be detected in BGO detectors (further described in section 2.4) placed on the opposite side. From the measured intensities in the detectors, the attenuation in the fuel assembly can be calculated and hence the void can be educed. The measuring table is shown in Figure 2.2.

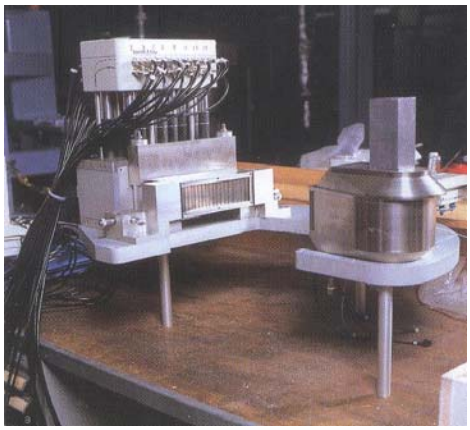

Figure 2.2. The FRIGG loop tomographic measuring table. Reproduced by courtesy of Westinghouse Electric Sweden AB.

The measuring geometry is illustrated in Figure 2.3. The system consists basically of an instrumentation table carrying a gamma source and 16 gamma-ray detectors, placed in two rows. The table can be rotated 200° about the fuel assembly. The measured intensities in a certain angle make up a gamma-ray intensity projection. Each projection can be more fully covered by a possibility to rotate the detectors 1.2° about the source. This way, the gamma-ray transmission through the assembly can be registered in a large number of different positions. One tomographic measurement at FRIGG is based on transmission data in about 17 000 positions.

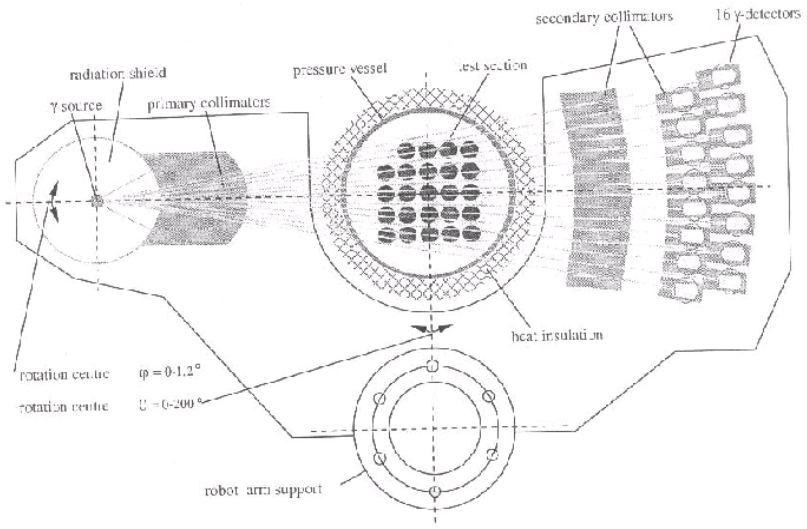

Figure 2.3. Void measuring system at FRIGG, ref. [2].

2.4 The BGO gamma radiation detector

The BGO or bismuth germanate detector, which is used for the void measurements at FRIGG, is a scintillation detector made of bismuth germanate crystal. When gamma quanta hit the detector, their deposited energies cause photon emissions in the crystal. The emitted light is then converted to electric pulses with amplitudes proportional to the deposited energies of the quanta. The pulses can be used to construct an energy spectrum. Gamma quanta that deposit all their energy to the detector will end up in the full energy-peak in the spectrum while quanta that deposit only part of their energy end up at a lower energy. The energy resolution of the BGO-detector is relatively low. An energy spectrum of the 662 keV gamma radiation from Cs-137, obtained using a BGO detector is shown in Figure 2.4.

2.5 Data acquisition system at FRIGG

At FRIGG, the data acquisition system is based on a pulse-height discriminator connected to a counter. The discriminator levels are set so that the full-energy peak of Cs-137 at 662 keV is selected, as illustrated in Figure 2.4. This acquisition technique implies that the counted pulses will include some background under the peak. The background consists of two components. Firstly of gamma quanta not depositing all their energy in the detector and secondly of gamma quanta that have lost some of their energy by interacting in the object.

The background in combination with the low energy resolution of the BGO detector also make it difficult to determine where the delimitation between energy peaks and background noise should be set, i.e. which discriminator settings are to be made. The settings decide the energy range within which quanta hitting the detector are counted.

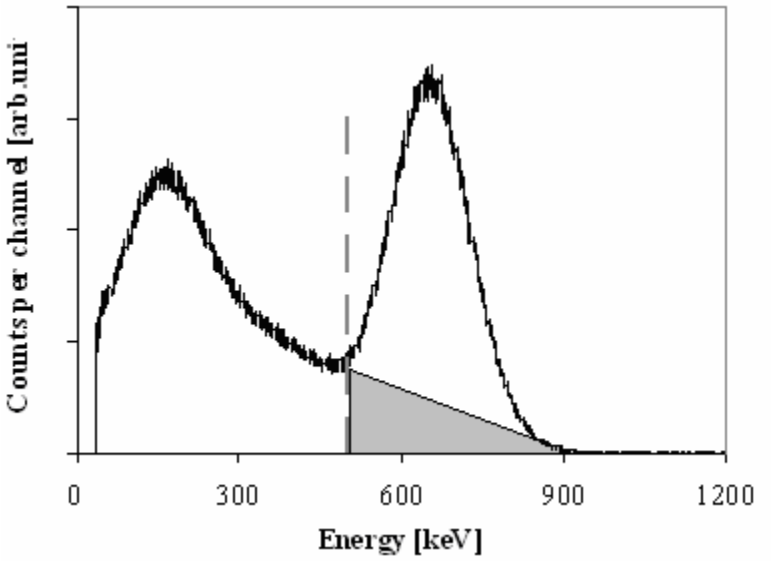

Figure 2.4. Gamma-ray spectrum of the 662 keV radiation from Cs-137 collected with a BGO detector. A possible setting of the lower discriminator level is also illustrated (from ref [3]). This type of data acquisition implies that the measured data will include background below the peak illustrated by a shaded triangle in the figure.

2.6 Earlier tomographic reconstructions of data from FRIGG measurements

Tomographic reconstructions of the void distribution from measured data have been made at Westinghouse Electric Sweden AB, using an analytic reconstruction technique, ref. [8]. Pictures from these reconstructions have been published in ref [9] and one of them is also reproduced in Figure 2.5. In this picture, the attenuation coefficient has been transformed into describing the void as described in section 3.6. In the picture, black colour corresponds to zero void, i.e. pure water (and also rod or box material), and white colour corresponds to 50% void.

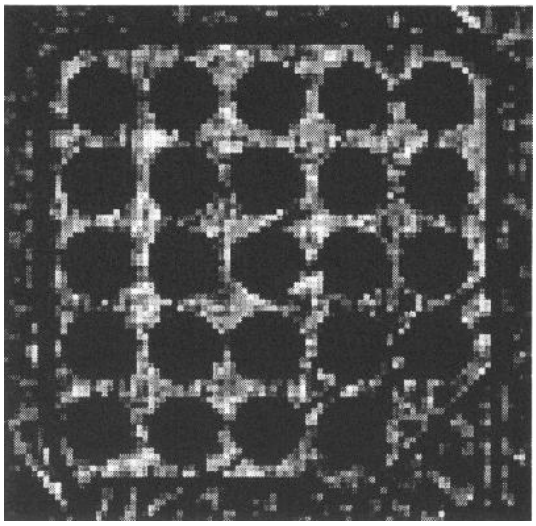

Figure 2.5. An example of a picture of the void distribution reconstructed by Westinghouse. Reprinted by courtesy of Westinghouse Electric Sweden AB.

2.7 Scope of this work

The purpose of this diploma work has been to investigate the possibility to increase the resolution and the precision in pictures of the void distribution, reconstructed from data achieved in tomographic measurements made at FRIGG, by using an algebraic reconstruction technique. The particular technique used is described in section 3.

One advantage with using the suggested technique is that the value of the attenuation coefficient in regions with material of well-known properties can be set. Accordingly, these regions may be excluded in the reconstruction. The possibility to use this advantage to increase the resolution of the pictures reconstructed from the FRIGG measurements has been investigated in section 5.

3 Tomographic reconstruction technique

The computer code for making the reconstructions in this work was written in the programming language Fortran90. At the Department of Radiation Sciences at Uppsala University, software has been developed for calculating gamma-ray travel distances through nuclear fuel assemblies, for the purpose of emission tomography, ref. [3]. This software was at disposal also for this project. Parts of the software could be rewritten to fit transmission tomography and could thereby be used for processing the FRIGG measurements.

3.1 Algebraic reconstruction

The measured intensities in the detectors depend on the distances the gamma rays travel in different materials and the attenuation coefficient of each material. The measured intensity can be expressed using the following equation:

$$I = I_0 e^{-\int \mu(t)\,dt} \qquad \textbf{Eq. (3.1)}$$

where I is the measured intensity in the detector,
I_0 is the intensity that would be measured if no material would be present between the source and the detector, here also called the reference intensity,
t is the position along the gamma ray,
$\mu(t)$ is the attenuation coefficient at position t.

Rewriting this equation using a logarithm and a discrete form of the integral leads to the following expression:

$$\ln\left(\frac{I}{I_0}\right) = -\sum \mu(t)\cdot \Delta t \qquad \textbf{Eq. (3.2)}$$

In this case, the measured gamma-ray intensities in a tomographic measurement form a system of equations where the relative intensities can be expressed in terms of attenuation and distances through different parts of the fuel assembly. Writing the equation on matrix form gives:

$$\begin{pmatrix} \ln\left(I_1/I_0\right) \\ \ln\left(I_2/I_0\right) \\ \cdot \\ \cdot \\ \ln\left(I_M/I_0\right) \end{pmatrix} = -\begin{pmatrix} t_{11} & t_{12} & \cdot & \cdot & t_{1N} \\ t_{21} & \cdot & & & \cdot \\ \cdot & & \cdot & & \cdot \\ \cdot & & & \cdot & \cdot \\ t_{M1} & & & & t_{MN} \end{pmatrix} \begin{pmatrix} \mu_1 \\ \mu_2 \\ \cdot \\ \cdot \\ \mu_N \end{pmatrix} \qquad \textbf{Eq. (3.3)}$$

Here it has been assumed that the fuel assembly has been divided into N picture elements, or pixels, and that the intensity has been measured in M different positions.

The intensities I and I_0 are measured in FRIGG and the distances t_{mn} are calculated. Accordingly, the μ-values can be determined numerically by solving the system of equations. In this work, this is done algebraically using the ASIRT method.

3.2 The ASIRT method

There are a number of different algebraic methods that can be used in tomographic reconstruction. Here, the ASIRT method is being used, since convergence is easily obtained with this algorithm. Furthermore, it has a small condition number and is hence often stable, ref [4]. The formula for solving Eq. (3.3) using the ASIRT method reads:

$$\mu_j^{k+1} = \mu_j^k + \frac{1}{\sum_{i=1}^{M} t_{ij}} \sum_{i=1}^{M} \frac{\left(\ln\left(\frac{I_i}{I_0}\right) - \sum_{j=1}^{N} t_{ij}\mu_j^k \right) t_{ij}}{\sum_{j=1}^{N} t_{ij}} \qquad \textbf{Eq. (3.4)}$$

where μ is the calculated attenuation coefficient,
t is the distance traveled by the gamma ray,
I_i is the measured value of the intensity and
I_0 is the reference value of the intensity

The ASIRT method is additive. It can be noted that the term $\ln\left(\frac{I_i}{I_0}\right) - \sum_{j=1}^{N} t_{ij}\mu_j^k$ is the difference between measured and calculated intensities and is used as correction term according to Eq. (3.4)

3.3 The picture

In this work, the picture consists of quadratic picture elements, or pixels. A picture based on quadratic pixels is conceptually illustrated for one fuel rod in Figure 3.1.

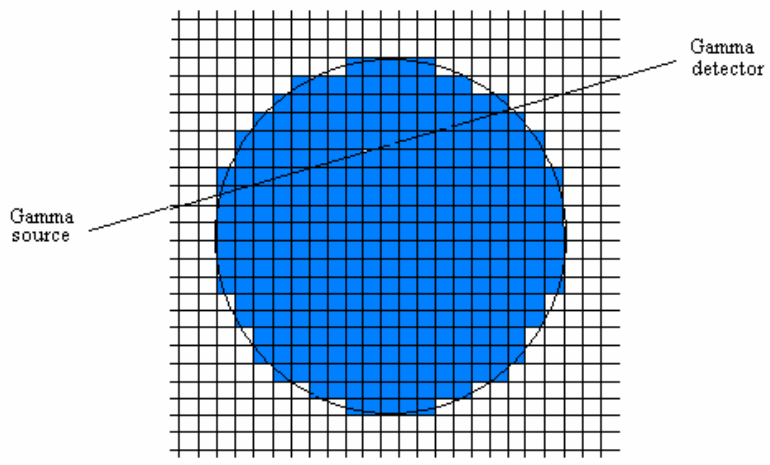

Figure 3.1. A principal sketch of quadratic pixel pattern covering one fuel rod.

One disadvantage using quadratic pixels is that pixels at the edges of the fuel rods will cover areas consisting of both water and rod material, as illustrated in Figure 3.1. Using this approach, pixels where the center point is inside a rod will be considered as covering fuel material, and pixels where the centre is outside the rod will be considered as covering water. This will, however, give an irregular shape of the pattern at the edges of the rods. It can be noted that this problem also occurs for other construction material and geometries in the picture.

Because a quadratic pixel pattern consists only of horizontal and vertical lines, the calculations using this approach can be based on a two-dimensional coordinate system, as illustrated in Figure 3.2.

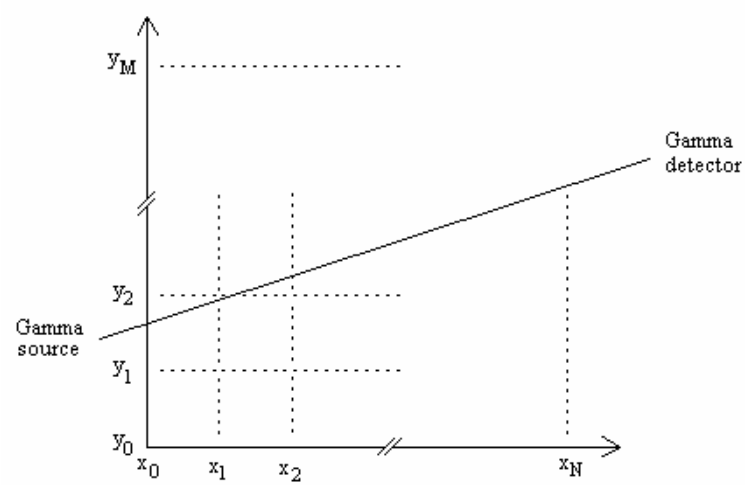

Figure 3.2. A schematic illustration of a coordinate system defining a quadratic pixel pattern.

In the calculations using this approach, every coordinate (x,y) where a gamma ray crosses a horizontal or vertical line will be determined. Using these coordinates, all distances traveled by the ray in different pixels, coefficients t_{mn} of Eq. (3.3), can be extracted.

3.4 Resolution

The achievable resolution of the reconstructed picture depends on the number of measured intensities. For the system of equations to give a unique solution, the number of measured intensities must be larger than the number of pixels in the picture. See Eq. (3.3).

3.5 Taking known geometric information into account

It can be noted that the attenuation coefficients in some materials are relatively well known. Such materials are the fuel rods, the fuel channel and the pipe surrounding the assembly. This information can be used to reduce the number of unknown parameters in Eq. (3.3). The gamma-ray travel distances through the well-known objects, as illustrated in Figure 3.1, can be calculated and the corresponding loss of gamma-ray intensity can be subtracted from the logarithm of the intensity measured in the detectors (left-hand side of Eq. (3.3)). Accordingly, by modelling the fuel, the attenuation in the fuel rods can be subtracted, whereas pixels covered by the fuel rods can be excluded from the reconstruction. This gives a smaller number of unknown parameters in the equation system.

However, the idea of this work is that instead of reducing the number of unknown parameters, the spatial resolution of the reconstructed image may be increased. Since nearly 50 % of the area inside the fuel channel consists of fuel rods with known properties, as can be seen in Figure 1.1, a substantial increase in resolution should be achievable. This is further discussed in connection with the presentation of the results in section 5.2.2.

3.6 Translating attenuation coefficients into void data

To produce pictures describing the void distribution instead of the attenuation coefficients, some calculations need to be made. Since the measured attenuation coefficient value is directly proportional to the mean density of the steam and water mixture through which the gamma-ray is traveling, it can be described using Eq. (3.5). See also ref [2].

$$\overline{\rho} = \alpha\rho_s + (1-\alpha)\rho_w, \qquad \textbf{Eq. (3.5)}$$

where $\overline{\rho}$ is the mean density of the mixture, ρ_s is the density of the steam, ρ_w is the density of the water and α denotes the volume fraction of the steam, i.e. the void.

The void is then given by Eq. (3.6).

$$\alpha = \frac{\mu_w - \overline{\mu}}{\mu_w - \mu_s}, \qquad \textbf{Eq. (3.6)}$$

where the calculated value of the attenuation coefficient is denoted by $\overline{\mu}$ and the indices w and s refer to water and steam, respectively.

4 Evaluated data sets

In this work, both simulated and measured data have been evaluated and analysed.

4.1 Simulated data

Simulated data is very useful when evaluating a new analysis technique because it contains no unknown factors. The software used for obtaining simulated data in this work was the established Monte Carlo code for particle transport, MCNP, ref [6]. It has earlier been used for investigating the feasibility of neutron radiation for void measurements, ref [5]. In the current work, it was used to simulate gamma radiation passing through an artificial fuel assembly. 99 detectors positions were used in 269 projections, which gives a total of 26 631 data points. The transmission of exactly 100 000 particles was simulated from the source to each detector. Due to the attenuation, only a fraction of these hit the detectors. In the simulations, the events where no interaction had occurred in the object were chosen. This implies that no consideration needs to be taken to scattering of particles when reconstructing the pictures.

It should be noted that the simulated data will include statistical noise. In these simulations, the relative standard deviation in each data was below 1%, ref [5].

The simulations were performed for a similar geometry as in the FRIGG measurements, with a fuel object including 24 rods surrounded by water. The fuel radius was here 6.125 mm and the distance between the centers of the rods was 16.30 mm. The rods were assumed to be homogeneous and made of iron. In the simulations, water cylinders with a radius of 4 mm having 60 % of the normal water density were placed at nine different locations, simulating void between the fuel rods. These areas are shown as circles of a brighter colour in the schematic picture of the simulated fuel assembly presented in Figure 4.1.

The attenuation coefficient in each simulated material is accounted for in Table 4.1.

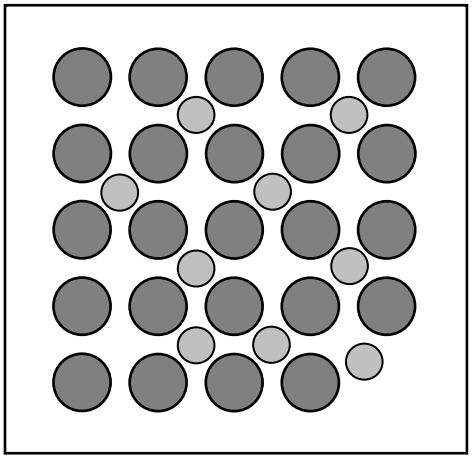

Figure 4.1. A schematic picture of the sub bundle used in the simulations. In the water surrounding the rods, nine cylinders with 60 % density were placed, simulating void.

Material	**Attenuation coefficient** [mm^{-1}]
Rods (iron)	0.0579
Water	0.00856
Water (60% density)	0.00514

Table 4.1. The attenuation coefficient values used in the simulations.

4.2 Measured data

In the FRIGG measurements, the number of gamma particles hitting the detector was recorded for 112 detector positions in 153 projections, making in total 17 136 positions. Before and after a void measuring session, a calibration measurement was performed. The calibration values were, in the evaluation of data, used as reference intensity values, see Eq. (3.3). The calibration procedure is more elaborately described in section 4.3.

The measurements were made on a sub bundle illustrated in Figure 4.2. There are 24 rods in the sub bundle and each rod has an inner diameter of 8.22 mm and an outer diameter of 9.62 mm. They consist of boron nitride surrounded by cladding. A heater is also placed inside the rods, as shown in Figure 4.3. The distance between the centers of two rods is 12.70 mm.

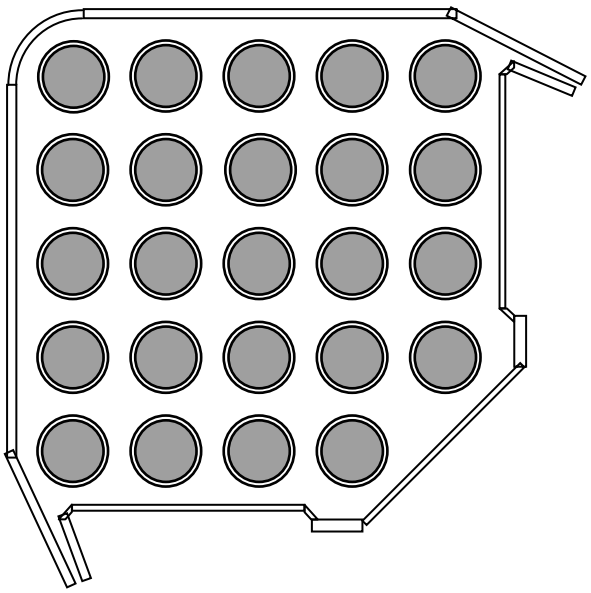

Figure 4.2. A schematic picture of a sub bundle that is being tested in FRIGG.

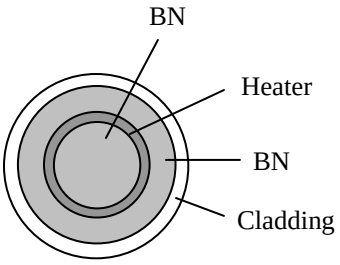

Figure 4.3. A cross section of a mockup rod used in FRIGG.

The values of the attenuation coefficient of 662 keV gamma radiation in different materials in the fuel mockup are accounted for in Table 4.2.

Material	**Attenuation coefficient** [mm^{-1}]
Pipe	0.0580
Isolation	0.000762
Water	0.00679
Cladding	0.0635
Boron	0.0147
Heater	0.0621
Steam	0.000309

Table 4.2. The attenuation coefficients of 662 keV gamma radiation in different material in the fuel mockup.

4.3. Reference intensities

The use of reference intensities I_0, corresponding to the measured intensity if no material would be present between the source and the detector, is crucial for the reconstruction technique presented in section 3.1. In the simulations, reference values of the intensity were obtained by performing a simulation without any object present. However, such a measurement could not be performed at FRIGG, because the counting rate of the non-shielded detectors would have been unacceptably high. Instead, a slab was placed between the source and the detector. In this work, several assumptions have had to be made regarding the calibration time and the slab geometry. Assuming the slab had the shape of a rectangle, the traveling distance through the slab would have varied for the different detectors depending on the angle between the source and the detector. See Figure 4.4. In FRIGG, calibration measurements were made twice for each of the sixteen detectors, once before and once after the tomographic measurement session was carried through.

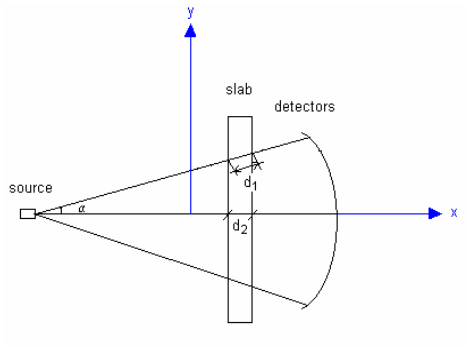

Figure 4.4. An illustration of the traveling distances of gamma-rays through a calibration slab.

The shortest way a gamma-ray could possibly travel through the slab is d_2, equal to the thickness of the slab. At an angle α, according to Figure 4.4, the distance through the slab is

$$d_1 = \frac{d_2}{\cos\alpha} \qquad \textbf{Eq. (4.1)}$$

Numerically, the maximal value of d_1 in FRIGG is $1.02 \cdot d_2$ for an angle α of 11°. It can be noted that a two-percent difference in the detector signal corresponds to the attenuation in 3 mm water in the FRIGG loop. Accordingly, such a systematic feature of the calibration has to be accounted for in the analysis.

In absence of information about the slab, it was assumed to have a rectangular shape. According to Eq. (4.1), the detected calibration intensities should differ depending on the distances the different gamma-rays travel through the slab. In addition, the calibration data can be divided into two sets, depending on the distance from the source. This is illustrated in Figure 4.5. A principal sketch of the expected features of the calibration data for this setup is shown in Figure 4.6.

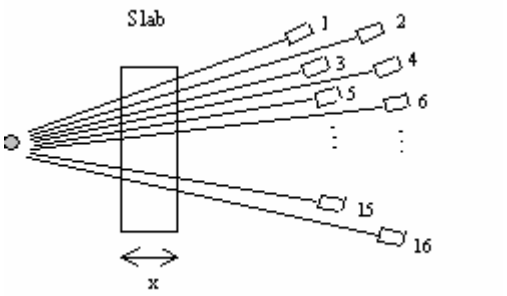

Figure 4.5. Gamma-ray distances through the slab at calibration.

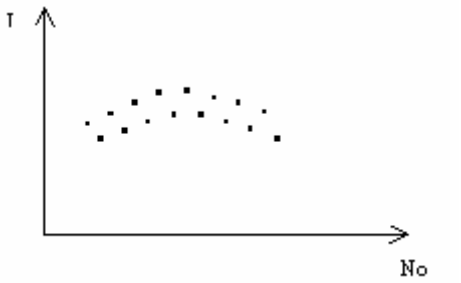

Figure 4.6. A principal sketch of the calibration data for the setup in Figure 4.5.

A plot made of the actual calibration data is shown in Figure 4.7.

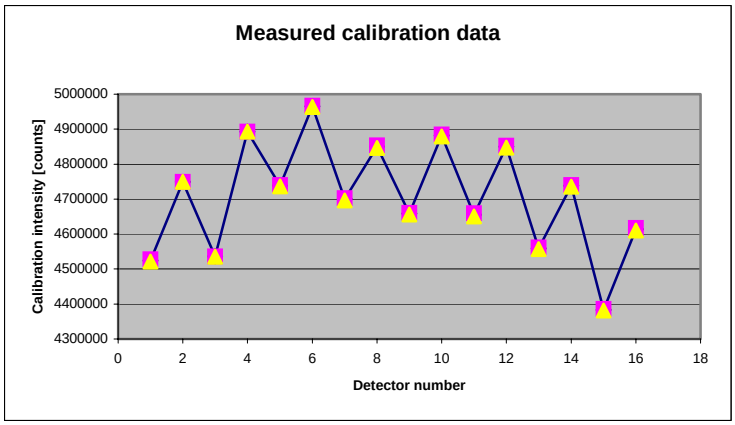

Figure 4.7. Plot of measured calibration intensities

The plot indicates that the assumptions made regarding the slab geometry were correct. With this knowledge, estimations of the attenuation in the slab could be made as is described below.

The intensity of the ray is proportional to $e^{-\mu x\frac{1}{\cos\alpha}}$ (see Figure 4.4). Note that, since the detectors are placed in two rows, as described in section 2.3, the calibration intensity values have to be divided into two populations depending on the distance to the source. In order to extract the attenuation through the shortest distance through the slab, i.e. the slab thickness x, the quotient of two ray intensities within the same data set is formed:

$$\frac{I_i}{I_j}=\frac{I_0 e^{-\mu\frac{x}{\cos\alpha_i}}}{I_0 e^{-\mu x\frac{1}{\cos\alpha_j}}}=e^{\mu x\left(\frac{1}{\cos\alpha_j}-\frac{1}{\cos\alpha_i}\right)} \qquad \textbf{Eq. (4.1)}$$

The logarithm of the expression above is

$$\ln\left(\frac{I_i}{I_j}\right)=\mu x\left(\frac{1}{\cos\alpha_j}-\frac{1}{\cos\alpha_i}\right), \qquad \textbf{Eq. (4.2)}$$

which the gives an expression for the attenuation in the shortest distance through the slab as follows:

$$\frac{\ln\left(I_i/I_j\right)}{\frac{1}{\cos\alpha_j}-\frac{1}{\cos\alpha_i}}=\mu x \qquad \textbf{Eq. (4.3)}$$

In the analysis, all odd-numbered detectors have been related to detector #1 and all even-numbered detectors to detector #16.

Results of calculated μx are shown in Figure 4.8.

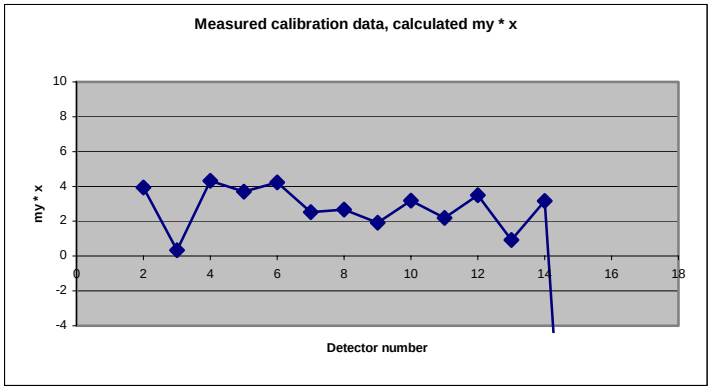

Figure 4.8. Plot of the calculated attenuation in slab, obtained in the analysis of calibration data.

Because of individual differences in the detector response, the values obtained are relatively spread. In this work, the mean value has been selected, which was μx = 2.8. Assuming that the slab was made of steel, this corresponds to a thickness of 50 mm.

In accordance with the above discussion, the measured calibration intensities were corrected with a factor $e^{\mu x \frac{1}{\cos \alpha_i}}$, where α_i is the angle to detector number i, as illustrated in Figure 4.4.

5 Results

Reconstructions have been made using both measured and simulated data. All resulting pictures have been presented in grey-scale images. The resolution, as well as the grey level schemes, has been varied. The pictures were created from reconstructed data using an image-analysing program created in a former degree thesis at the Department of Nuclear and Particle Physics at Uppsala University, ref [7].

5.1 Reconstructions using simulated data

5.1.1 Selection of grey-scale levels

The first reconstructions using simulated data were performed using a resolution of 50x50 pixels. The ability to reproduce the nine cylinders where the water density was lower, simulating void, was studied, see section 4.1. It was noted that, by setting appropriate discriminator levels in the picture, the range of the presented data values could be narrowed down to the range of interest. In this case, this region would be about 0.0051 mm^{-1} (simulated void) and 0.0086 mm^{-1} (water). Different discriminator levels were tried in the simulated pictures and some results are shown in Figures 5.1, 5.2, 5.3 and 5. 4 below. In the images, black colour represents the highest attenuation present and white colour represents the lowest. Note that these images show the attenuation in contrast to the image presented in Figure 2.5, showing the void.

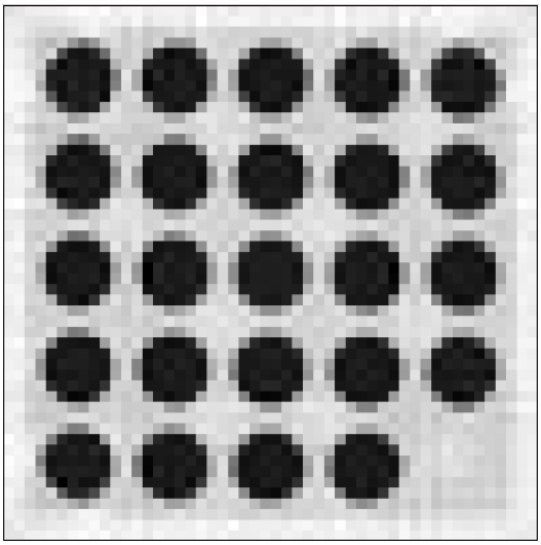

Figure 5.1. The result of a reconstruction of simulated data where no discriminator level was set in the picture. The nine regions with lower water density can not be identified.

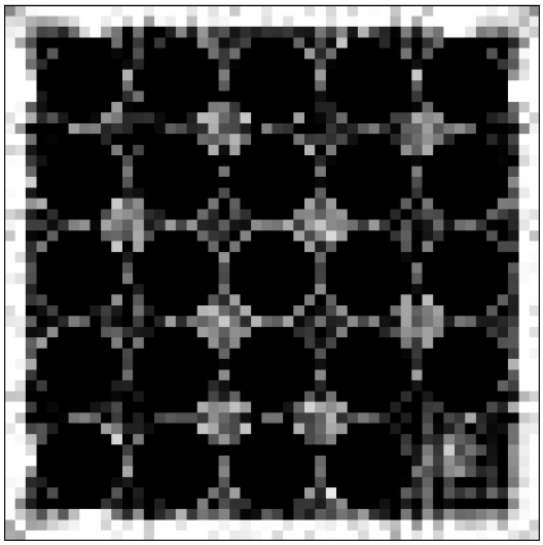

Figure 5.2. The result of a reconstruction of simulated data where the discriminator levels were set to 0 mm^{-1} (white) and 0.01 mm^{-1} (black). Here, it is possible to identify the nine regions with lower water density.

In the image where no discriminator levels were set, presented in Figure 5.1, the nine areas where the water density was lower can not be distinguished. The attenuation coefficient values are here in the range between -0.004 mm^{-1} and 0.07 mm^{-1}. The non-realistic negative values occur due to statistical noise in the simulations. With a lower discriminator level set on zero attenuation and the upper level set on 0.01 mm^{-1}, the simulated void areas can be distinguished, although with some difficulty, as shown in Figure 5.2. An image where the lower level is set to 0 mm^{-1} and the upper level is set to 0.006 mm^{-1}, is shown in Figure 5.3, whereas figure 5.4 shows an image where the lower level is set on 0.004 mm^{-1}, and the upper is set on 0.01 mm^{-1}. In both the latter cases, the areas with lower water density simulating void, as discussed in section 4.1, may be distinguished.

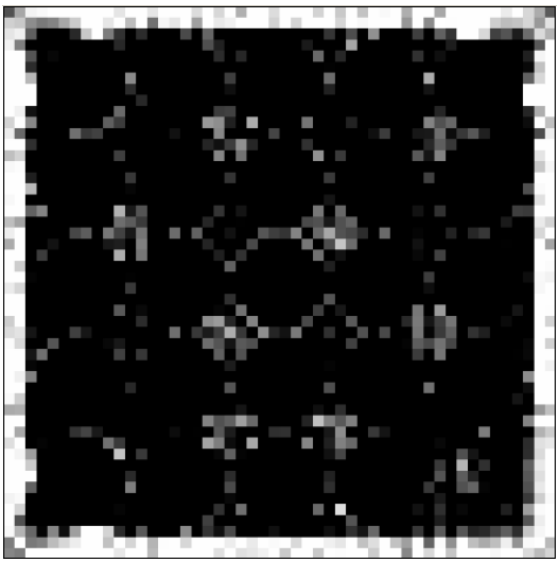

Figure 5.3. A reconstructed picture where the discriminator levels were set on 0 mm^{-1} and 0.006 mm^{-1}.

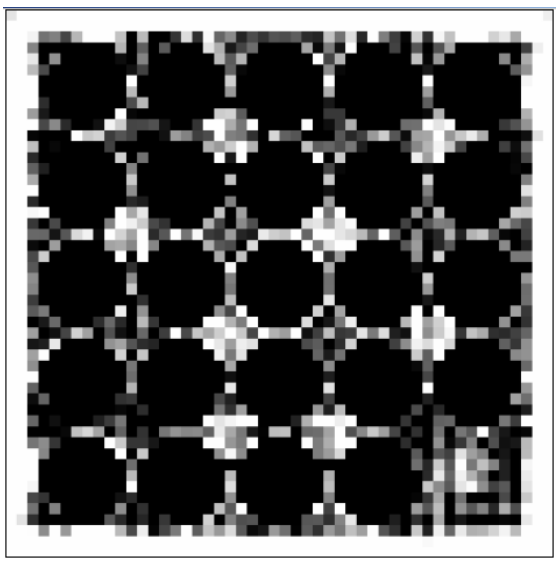

Figure 5.4. A reconstructed picture where the discriminator levels were set on 0.004 mm^{-1} and 0.01 mm^{-1}.

From the results shown in the pictures above, it can be seen that the discriminator levels play an important role when presenting the reconstructed pictures. The difference in attenuation coefficient values between the mockup rods and the surrounding water is much larger than the difference in attenuation coefficient values between the water and the simulated void areas. Since the areas of investigation contain water and steam, the range of the attenuation values of interest is therefore quite narrow. Based on this discussion and the results shown above, the following images will be presented using a lower discriminator level of 0 mm^{-1} and an upper level of 0.01 mm^{-1}.

5.1.2 Resolution in reconstructions using simulated data

Pictures with different resolution were also reconstructed using simulated data. Presented in Figures 5.5 and 5.6 below are results from simulations with 50x50 pixels and 80x80 pixels, respectively. Note that these images show the attenuation in contrast to the image presented in Figure 2.5, showing the void.

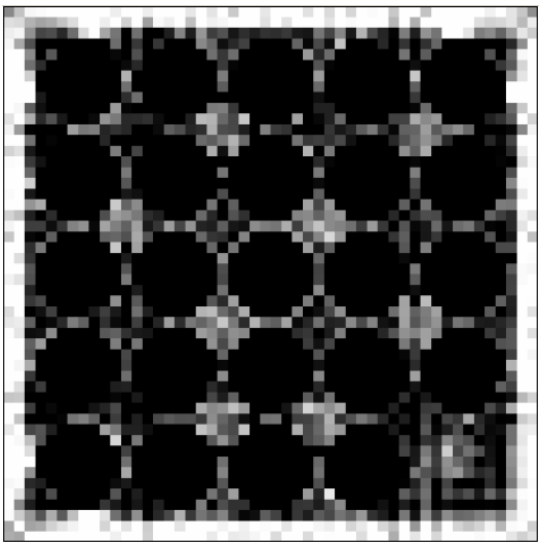

Figure 5.5. A reconstruction of simulated data with a resolution of 50x50 pixels. The discriminator levels were set on 0 mm^{-1} and 0.01 mm^{-1}.

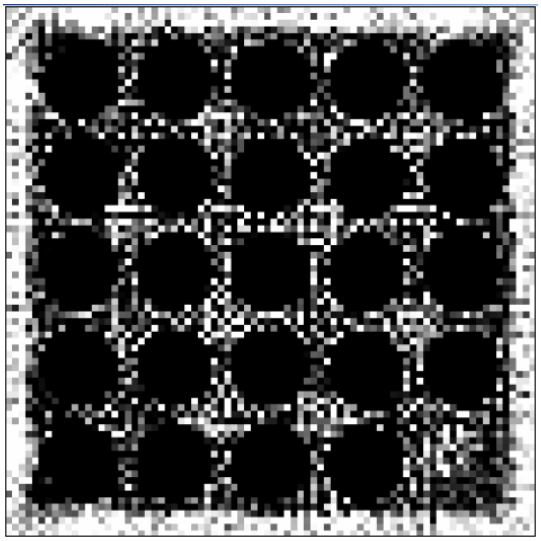

Figure 5.6. A reconstruction of simulated data with a resolution of 80x80 pixels. The discriminator levels set on 0 mm^{-1} and 0.01 mm^{-1}.

In the picture including 80x80 pixels, the simulated void areas can hardly be seen while they are more easily detected in the picture including 50x50 pixels. This indicates that the system of equations (see section 3.1) needs to be greatly over determined to avoid unacceptably high levels of noise in the resulting images.

5.2 Reconstructions using measured data

5.2.1 Basic reconstructions

Basic reconstructions, where no assumptions were made regarding known fuel geometries, have been performed from measured data, using an image resolution of 50x50 pixels and 80x80 pixels. The resulting images are presented in Figures 5.7 and 5.8. The grey-scale covers attenuation coefficients between 0 and 0.01 mm^{-1}.

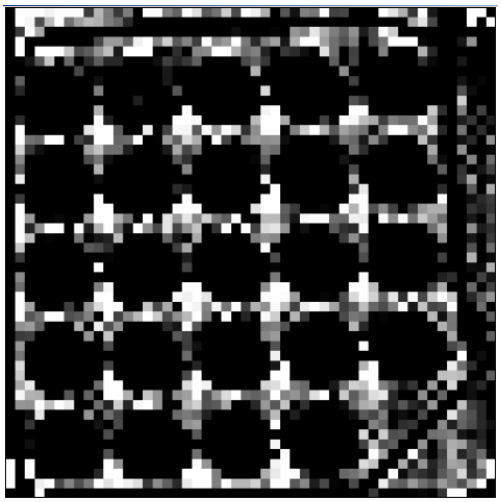

Figure 5.7. A reconstructed picture using measured data with a resolution of 50x50 pixels. The discriminator levels were set on 0 mm^{-1} and 0.01 mm^{-1}.

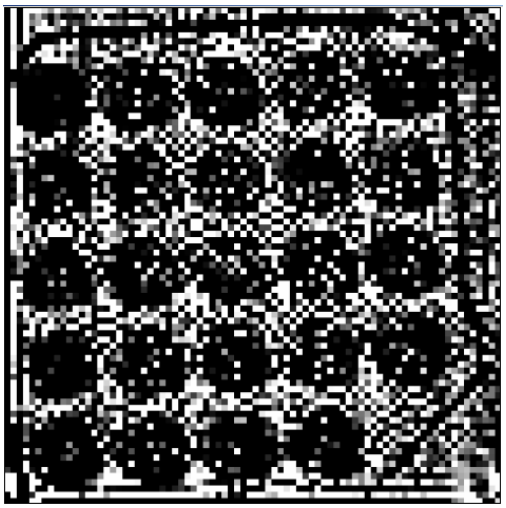

Figure 5.8. A reconstructed picture using measured data with a resolution of 80x80 pixels. The discriminator levels were set on 0 mm^{-1} and 0.01 mm^{-1}.

The same tendencies can be seen in reconstructed images from measured data as in the pictures from the simulations (see section 5.2.1). The resolution of 80x80 pixels, shown in Figure 5.8, seems to be too high, which leads to a high level of noise. The picture with a resolution of 50x50 pixels, on the other hand, shown in Figure 5.7, is reconstructed using a well over determined system of equations (see section 3.3) and hence the image is reasonably clear.

5.2.2 Subtraction of the attenuation in the rods

One of the ideas of this work was to present images with a higher resolution than earlier presented by taking into consideration the values of the attenuation coefficients of known geometries and hence get an equation system that is over determined enough also in reconstructions with high resolution, as described in section 3.4.

When subtracting the attenuation in the rods, it is crucial to know the exact position of the fuel. Therefore, the position of the fuel was determined using special-purpose software for analysing images of nuclear fuel, ref [7]. The analysis of the image presented in Figure 5.7 resulted in the following position of the fuel:

$x = -1.26$ mm
$y = -1.68$ mm
$\alpha = 2.12°$

The denotations are explained in Figure 5.9. The fuel assembly was modelled in this position and the attenuation in the rods was subtracted from Eq. (3.3), resulting in the reconstructed images presented in Figures 5.10 and 5.11.

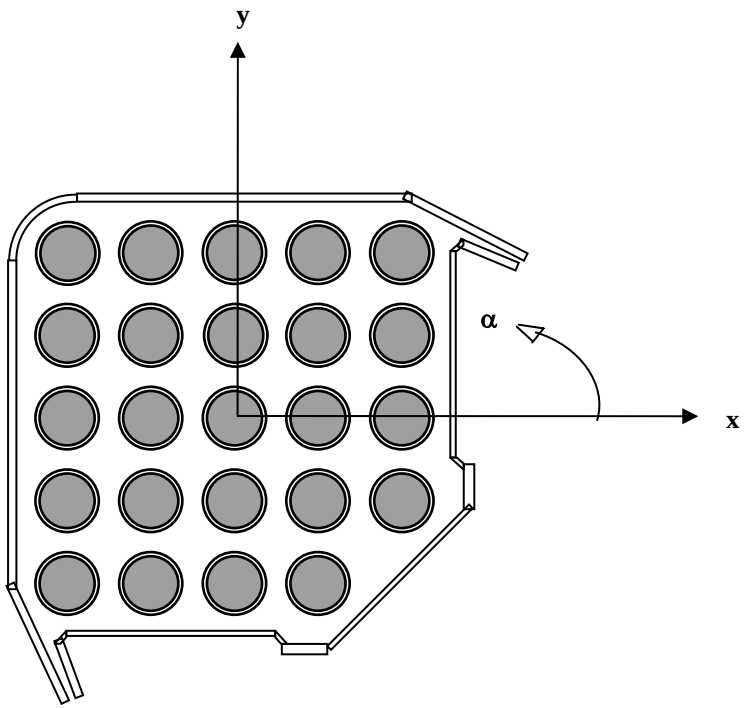

Figure 5.9. A schematic view of the coordinate system used when defining the fuel position of the fuel assembly tested in FRIGG.

Some of the results from the reconstructions where the attenuation in the rods has been subtracted are shown in Figures 5.10 and 5.11 below.

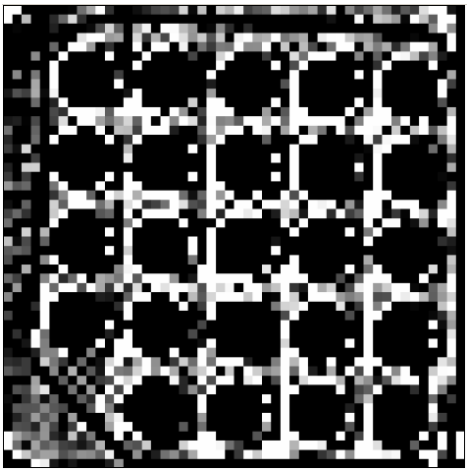

Figure 5.10. A reconstruction of measured data where the attenuation in the rods has been subtracted. The resolution is 50x50 pixels and the grey-scale level scheme goes from 0 to 0.01 mm^{-1}.

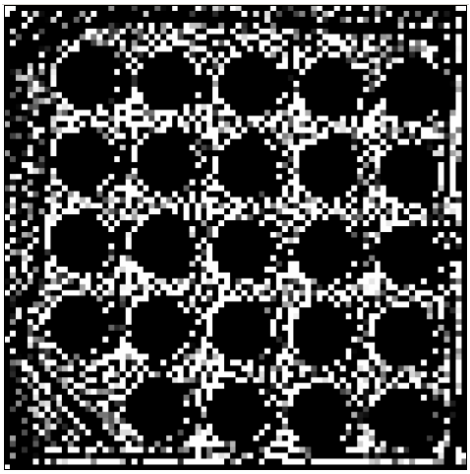

Figure 5.11. A reconstruction of measured data where the attenuation in the rods has been subtracted. The resolution is 80x80 pixels and the grey-scale level scheme goes from 0 to 0.01 mm^{-1}.

In Figure 5.11, it can be seen that subtracting the attenuation in the rods appears to give improved picture quality as compared to the basic reconstruction, shown in Figure 5.8. As an example, the area outside the box

encapsulating the rods, gets attenuation coefficient values that are more stable about the coefficient of water at 0.007 mm^{-1} , which is actually present in this area.

A similar improvement can, however, not be seen when comparing the pictures with 50x50 pixels presented in Figures 5.10 and 5.7. One explanation for this could be that the shape of the subtracted area is circular while the lattice used in the reconstructions is quadratic. Accordingly, the pixels cannot adapt properly to the fuel rods, which will introduce irregularities when subtracting the attenuation in the rod and excluding pixels only partly covering rods from the reconstruction. If the pixels are very large, the effect of this will become substantial, while it will be less prominent if smaller pixels are used.

5.2.3 Remarks

There is a considerable level of statistical noise in the reconstructed pictures. Two reasons why this noise arises have been identified:

The signal consists of a reduction in gamma-ray intensity as compared to a reference intensity. This reduction is mainly sensible to the fuel rod material, which has an attenuation coefficient about a factor ten larger than water. Uncertainties in the reconstruction of the fuel material will affect the surrounding water, which will obtain an unacceptably high relative level of noise.

Also, the attenuation in the surrounding pressure vessel has to be subtracted before performing a reconstruction, both using the algebraic technique suggested in this work and the analytic technique earlier used, ref. [8]. Because of the data-acquisition technique used, described in section 2.5, a significant contribution from scattered gamma quanta will be included in the data. This may be interpreted as a lower effective value of the attenuation coefficient. Since the settings are different for different detectors, it will be difficult to decide which value of the attenuation coefficient to select in this subtraction. The same problem arises when subtracting the attenuation of the rods. The problem might be solved using another calibration method than the one used in the FRIGG measurements. Such a method is suggested in section 5.3.

A solution to the problem with statistical noise could also be to use radiation more sensitive to the attenuation in water and void, e.g. using neutrons instead of gamma radiation or using a different type of calibration. Also in this case, the calibration method suggested in section 5.3 may be used.

5.3 Use of a reference data set

One way to make a more precise calibration could be to fill the assembly with water, using non-heated rods and make a full measurement session. This would lead to one reference intensity for every measurement point corresponding to the value obtained with no void present. Consequently, there would be no need to subtract the attenuation in the rods or in the regions outside the reconstructed image, which is presently required. Accordingly, a large source of uncertainty would be omitted, since the effective value of the attenuation coefficient depends highly on the detector settings in the present setup. The result of this type of measurement would be a picture showing the change in attenuation, as compared to the case with no void present. Simulations were performed with this type of calibration and the results are presented in Figures 5.13 and 5.14.

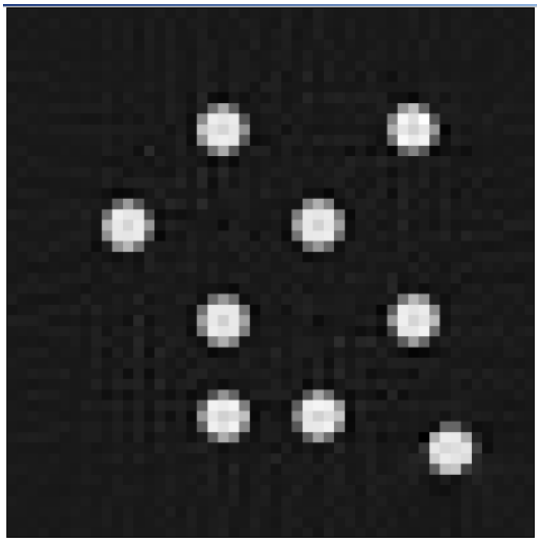

Figure 5.13. A reconstruction using simulated data where unique reference intensities for every measuring point were used. The resolution of the picture is 50x50 pixels.
The grey-scale covers attenuation differences between -0.004 mm^{-1} (white) and 0.0006 mm^{-1} (black).

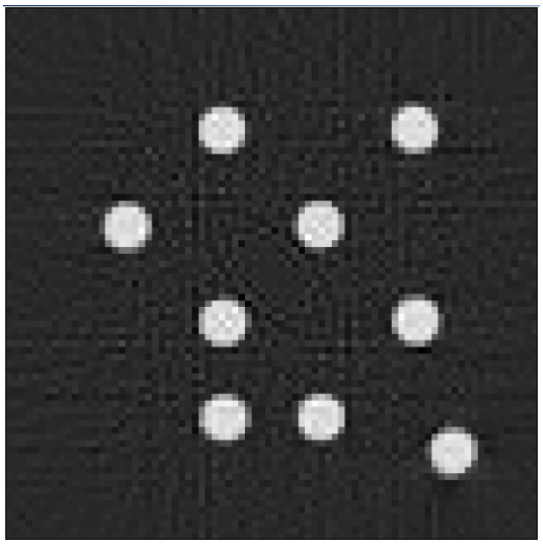

Figure 5.14. A reconstruction using simulated data where unique reference intensities for every measuring point were used. The resolution of the picture is 80x80 pixels.
The grey-scale covers attenuation differences between -0.004 mm^{-1} (white) and 0.0006 mm^{-1} (black).

In the pictures shown in Figures 5.13 and 5.14, it can be seen that the void areas are very prominent. Also, the value of the attenuation difference agrees with the reduction of 0.0034 mm^{-1} expected according to Table 4.1. This indicates that the calibration procedure discussed here could also be used for measured data. The practical implementation of this technique is further discussed in section 6.1.

It can be noted that, with calibrations made this way, the advantages of already known values of attenuation coefficients inside the fuel rods could still be used. Since the properties of the rods would be the same both during the calibration measurement and the main measurement session, the pixels in these areas could be considered having unchanged attenuation values and hence be set to zero in the reconstruction. Therefore, no calculations would have to be made in the areas enclosed in fuel rods. To test this technique, this type of reconstruction was also made. The reconstructed images from this simulation are shown in Figures 5.15 and 5.16.

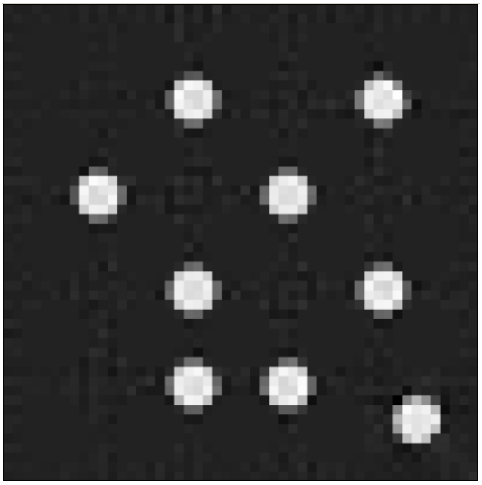

Figure 5.15. A reconstruction using simulated data and unique reference intensities for every data point. In this reconstruction, the difference in attenuation values of the rods was set to zero and such pixels were excluded in the reconstruction. The resolution of the picture is 50x50 pixels.

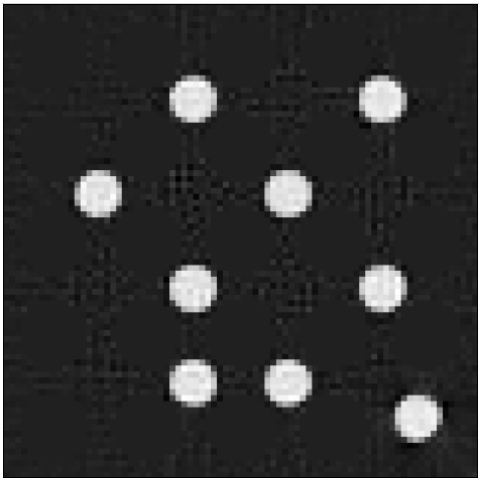

Figure 5.16. A reconstruction using simulated data and unique reference intensities for every data point. In this reconstruction, the difference in attenuation values of the rods was set to zero and such pixels were excluded in the reconstruction. The resolution of the picture is 80x80 pixels.

The results using this approach appears to give an even smaller level of noise than what was presented in Figures 5.13 and 5.14. This may be a result of the reduced number of pixels taking part in the reconstruction, leading to a more over determined equation system, see Eq. (3.3).

6 Outlook

In section 5.2.3 it was concluded that the tomographic measurements would benefit from an enhanced sensitivity to the water and void areas present in the fuel. Two suggestions of how to achieve this are discussed in sections 6.1 and 6.2 below. Also, a suggestion of a change in the pixel pattern is discussed in section 6.3.

6.1 Use of a reference set

An alternative technique for obtaining a reference intensity that is unique for every data point was suggested and investigated in section 5.3. If the calibrations were to be made using this method, the two measurement sessions, the reference measurements and the ordinary measurements, should preferably be measured close in time to the void measurements. This is to avoid variations in detector response with time.

If the calibrations are made this way, two pictures may be reconstructed. The first using only the void measurement data to get an image of the fuel, such as the image shown in Figure 5.1. The second image would be reconstructed using reference intensities, giving an image of the differences from the first image, such as the image shown in Figure 5.13. These two images together would then give a good view of the void distribution in the fuel. In Figure 6.1, an example of two images that could form the basis of such a view is presented.

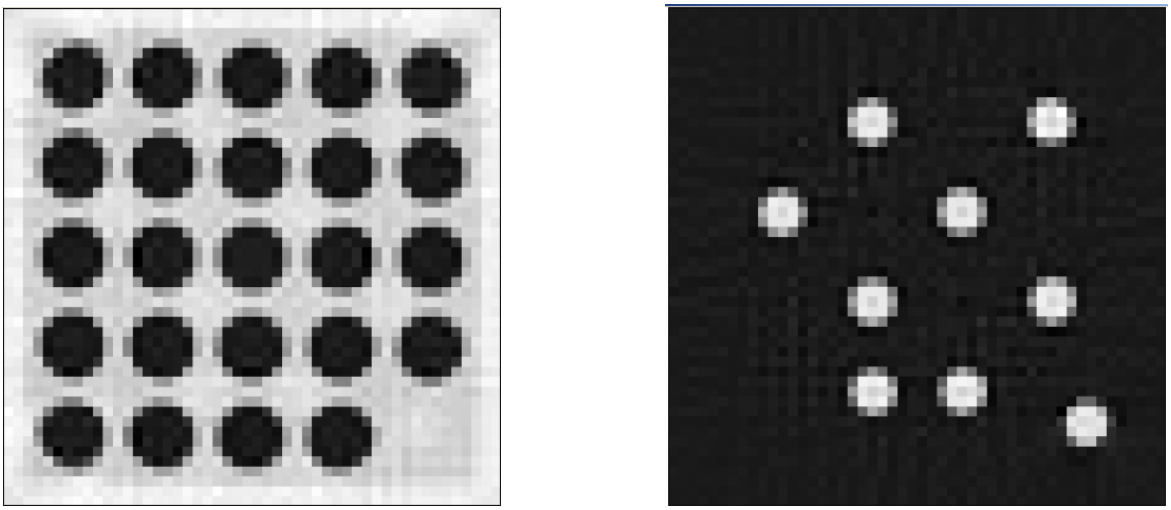

Figure 6.1. Using a combination of the images presented in the figure would give a well-informed view of the void distribution.

It would, however, be of greatest importance that the calibration measurement session is made in the exact same way as the rest of the measurements. This could imply some difficulties since the positioning of the equipment might not be that precise. Which level of precision that would be required has not been investigated in this work.

6.2 Neutron measurements

One way to make the measurements less sensitive to the attenuation in the rods and more sensitive to the attenuation in water, as discussed in section 5.2.3, would be to use neutrons instead of gamma radiation in the measurements. A simulation study of measurements performed this way has been done, ref. [5]. Still with measurements made with neutrons, the calibration technique suggested in section 5.3 may be used. Also, the fuel rods may be excluded from the reconstruction as described in sections 5.2.2 and 5.3.1.

6.3 Quadrangular pixels

Using quadrangular pixels, the reconstructed picture would be built up by pixels with four corners but, unlike in the case with quadratic pixels, with irregular sides, as illustrated in Figure 6.1. This type of objects have earlier been used in the software described in ref. [3].

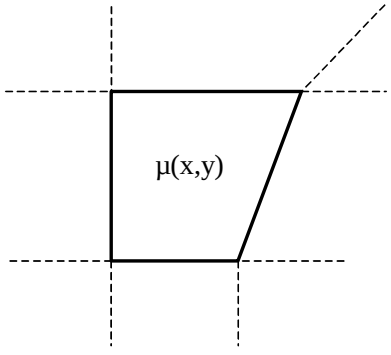

Figure 6.1. A principal sketch of a quadrangular pixel.

Basing the picture on this type of pixels would make the software flexible. The pixel forms could be adjusted to different geometrical shapes. With this approach, the same computational mesh as the one used in the thermal-hydraulics codes that are to be evaluated in FRIGG could be used.

7 Acknowledgements

First and foremost I would like to thank Staffan Jacobsson Svärd, my supervisor, who has been a tremendous help to me during my time with this project and Ane Håkansson who has been the academic reviewer of this thesis. I would also like to thank Stig A. Andersson and Leif H. Pettersson at Westinghouse who have given me a lot of support by sending me data and blueprints of FRIGG and letting me use their expertise. John Loberg has been a tremendous help to me by performing simulations for me to reconstruct and evaluate. Thank you also to Mats Troeng, who has helped me in my work with analysing the pictures. Last but not at all least, I have had a great time at the Department of Nuclear and Particle Physics thanks to the fantastic (and also pretty weird, but in a good way) people of this research group. It is really difficult to be in a bad mood around you!

9 References

1. *FRIGG Fullskaleprovning av bränslepatroner*, ABB Atom AB

2. Westinghouse Electric Sweden AB, proprietary information.

3. S. Jacobsson Svärd: *A Tomographic Measurement Technique for Irradiated Nuclear Fuel Assemblies*, Comprehensive Summaries of Uppsala Dissertations from the Faculty of Science and Technology 967, (2004).
   Available at http://urn.kb.se/resolve?urn=urn:nbn:se:uu:diva-4227

4. T. Lundqvist: *Investigation of Algebraic Reconstruction Techniques for Tomographic Measurements on Spent Nuclear Fuel Assemblies*, Uppsala universitet, (2004)

5. J. Loberg: *Investigation of void effects in boiling water reactor fuels using neutron tomography*, Uppsala universitet, ISSN 1401-6269, (2006)

6. J. F. Briesmeister: *MCNP – A General Monte Carlo N-Particle Transport Code – Version 4C*, Report LA-13709-M, Los Alamos National Laboratory, (2000).

7. M. Troeng: *Positioning of Nuclear Fuel Assemblies by Means of Image Analysis on Tomographic Data*, Uppsala universitet, ISSN 1401-5749, (2004)

8. Westinghouse Electric Sweden AB, proprietary information.

9. G. Windecker and H. Anglart: *Phase distribution in BWR fuel assembly and evaluation of multidimensional multi-field model*, ABB Atom AB, (1999). Presented at NURETH-9, San Fransisco, California, October 3-8 1999.S